Examination of Contrast Mechanisms in Optoacoustic Imaging of Thermal Lesions

Christian Richter[1,2], Gloria Spirou[1,3], Alexander A. Oraevsky[4], William M. Whelan[3,5] and Michael C. Kolios[3,5]

[1]Ontario Cancer Institute/Princess Margaret Hospital, Toronto, Canada;
[2] Faculty of Arts and Science, University of Toronto, Toronto, Canada;
[3]Department of Medical Biophysics, University of Toronto, Toronto, Canada;
[4]Fairway Medical Technologies, Inc., Houston;
[5]Department of Physics, Ryerson University, Toronto, Canada

ABSTRACT

Optoacoustic Imaging is based on the thermal expansion of tissue caused by a temperature rise due to absorption of short laser pulses. At constant laser fluence, optoacoustic image contrast is proportional to differences in optical absorption and the thermoacoustic efficiency, expressed by the Grüneisen parameter, Γ. Γ is proportional to the thermal expansion coefficient, the sound velocity squared and the inverse heat capacity at constant pressure. In thermal therapies, these parameters may be modified in the treated area. In this work experiments were performed to examine the influence of these parameters on image contrast. A Laser Optoacoustic Imaging System (LOIS, Fairway Medical Technologies, Houston, Texas) was used to image tissue phantoms comprised of cylindrical Polyvinyl Chloride Plastisol (PVCP) optical absorbing targets imbedded in either gelatin or PVCP as the background medium. Varying concentrations of Black Plastic Color (BPC) and titanium dioxide (TiO_2) were added to targets and background to yield desired tissue relevant optical absorption and effective scattering coefficients, respectively. In thermal therapy experiments, ex-vivo bovine liver was heated with laser fibres (805nm laser at 5 W for 600s) to create regions of tissue coagulation. Lesions formed in the liver tissue were visible using the LOIS system with reasonable correspondence to the actual region of tissue coagulation. In the phantom experiments, contrast could be seen with low optical absorbing targets (μ_a of $0.50cm^{-1}$ down to $0.13cm^{-1}$) embedded in a gelatin background ($\mu_a = 0.13cm^{-1}$ and $\mu_{s'} = 4.2cm^{-1}$). Therefore, the data suggest that small objects ($< 5mm$) with low absorption coefficients (in the range $< 1cm^{-1}$) can be imaged using LOIS. PVCP-targets in gelatin were visible, even with the same optical properties as the gelatin, but different Γ. The enhanced contrast may also be caused by differences in the mechanical properties between the target and the surrounding medium. PVCP-targets imbedded in PVCP produced poorer image contrast than PVCP-targets in gelatin with comparable optical properties. The preliminary investigation in tissue equivalent phantoms indicates that in addition to tissue optical properties, differences in mechanical properties between heated and unheated tissues may be responsible for image contrast. Furthermore, thermal lesions in liver tissue, ex-vivo, can be visualized using an optoacoustic system.

Keywords: Optoacoustic Imaging, Photoacoustic Imaging, Grüneisen Parameter, thermoacoustic efficiency, thermal expansion, thermal therapy, thermal lesion, image contrast, tissue boundary

1. INTRODUCTION

Optoacoustic signals in biological tissue are caused by a local temperature rise due to absorption of pulsed laser light.[1] The resulting pressure transients give rise to pressure waves with frequencies ranging from tens of kHz to tens of MHz which travel through the tissue and can be detected with a transducer placed at the tissue surface. The range of laser-induced ultrasonic frequencies depends on the laser pulse duration and optical properties of tissue. Optoacoustic imaging is based on time-resolved detection of optoacoustic signals generated under conditions of temporary pressure confinement followed by an image reconstruction utilizing radial back projection of

correspondence email: mkolios@ryerson.ca

Photons Plus Ultrasound: Imaging and Sensing 2006: The 7th Conference on Biomedical Thermoacoustics, Optoacoustics, and Acousto-optics, edited by A. A. Oraevsky, et. al
Proc. of SPIE Vol. 6086, 60861K (2006) • 1605-7422/06/$15 • doi: 10.1117/12.650692

corresponding velocity potential values.[2,3]

In recent years there has been considerable interest in biomedical applications of optoacoustic imaging. The main advantage of this technique for medical diagnostics is the combination of the high contrast generated by differential tissue optical absorption and the comparatively small ultrasound tissue attenuation. The effective detection depth of optoacoustic imaging can reach 7.5 cm,[4] considerably greater than detection depths for infrared optical techniques (∼1 cm)[5] and optical coherence tomography (∼3 cm).[6] The attenuation of ultrasound is much lower than the attenuation of scattered light. In addition optoacoustic imaging has the potential for improved contrast over conventional ultrasound imaging, since optical properties show greater variation than acoustic properties.

Optoacoustic methods have been applied to breast[6,7] and prostate[8] cancer imaging as well as for measuring tumor blood oxygenation in rat brains.[9,10] The technique has the potential for both structural and functional imaging, without requiring the use of a contrast agent. In addition optoacoustic imaging does not involve exposure to X-rays or magnetic fields as it is the case for computed tomography (CT) and magnetic resonance imaging (MRI). Furthermore it is well-suited for real-time imaging during treatments and it is less expensive than MRI or X-ray CT modalities.

Most studies concentrate on the contrast caused by differential optical absorption. In this work we also investigate image contrast caused by heat-induced changes in optical absorption and thermo-elastic properties of tissues as a result of tissue coagulation during thermal therapy.

2. MATERIALS AND METHODS

2.1. Theoretical Background

To understand the detected optoacoustic signal and image contrast, it is necessary to understand the physical principles which are responsible for the generation of the optoacoustic signal. Absorbed optical energy, E_{abs} [J/m^3], from a laser source yields a local rise in temperature, ΔT [^{o}C], generating a pressure transient ΔP [Pa] inside this tissue volume according to[11]:

$$\Delta P = \frac{1}{\gamma}\beta\Delta T = \frac{1}{\gamma}\beta\left(\frac{E_{abs}}{\rho C_V}\right) \tag{1}$$

where γ [Pa^{-1}] is the thermodynamic coefficient of isothermal compressibility, β [K^{-1}] thermal coefficient of volume expansion, ρ [g/m^3] is the mass density of the medium and C_V[J/gK] is the specific heat capacity at constant volume. Hence, this pressure rise is the result of an expansion caused by a transformation of the absorbed laser energy into heat. Equation (1) can be simplified by expressing $\beta/\left(\gamma\rho C_V\right)$ as the dimensionless, temperature-dependent factor which represents the fraction of thermal energy converted into mechanical stress, also known as the Grüneisen parameter, Γ.[11]

$$\Delta P = \Gamma E_{abs} = \Gamma\mu_a H \tag{2}$$

where E_{abs} is the product of the laser fluence, H [J/m^2] and the optical absorption coefficient μ_a [m^{-1}] of the medium at the wavelength of the laser light.

For the optoacoustic effect to occur with maximum efficiency and for optoacoustic images to posses desirable resolution, the duration time of a single laser pulse τ_L has to be much shorter than the stress relaxation time τ_{SR} (the time it takes for the sound to propagate through the portion of the irradiated volume to be resolved).[11] The time of stress relaxation is much shorter than the heat diffusion time (the time it takes takes for the heat to escape out of the irradiated volume). After the generation of the pressure transient, the attenuation and diffraction of acoustic waves need to be taken into account. In this work we assume that the acoustic attenuation is negligible. We also assume that we detect spherical acoustic waves, i. e. acoustic waves in the far diffraction zone. Mismatches in the acoustic impedance during the acoustic wave propagation influences the optoacoustic

signal by creating reflections. The transmission of acoustic waves through boundaries of tissues with different acoustic impedances is not included in equation (2).

The laser fluence H in equation (2) (and therefore the absorbed energy) is related to the position of the absorber in the medium. The profile of the laser fluence as function of the depth H(z) in a non-scattering media can be described with the Beer-Lambert law as an exponential attenuation with μ_a as attenuation factor. In diffuse media not only light absorption but also scattering is present. This causes an effectively higher absorption due to an increased duration and slower propagation of light in the media. Therefore in scattering dominated media the attenuation is characterized by the effective absorption coefficient[11]

$$\mu_{eff} := \sqrt{3\mu_a(\mu_a + \mu_{s'})} \tag{3}$$

where μ_s' [m^{-1}] is the reduced scattering coefficient. In media with comparable scattering and absorption values computer simulations such as Monte-Carlo-Simulations are used to calculate the light distribution.[12]

In this work the effect of the Grüneisen parameter Γ on image contrast was investigated by using phantoms with the same optical properties but different mechanical properties. Moreover, experiments have been performed with the goal to investigate whether enhanced scattering in the target area influences the amplitude of the pressure transients produced or if scattering only influences the attenuation of the laser fluence. Therefore targets with the same absorption coefficients μ_a but different scattering values $\mu_{s'}$ (see section 2.2) were used. Also targets with similar effective scattering μ_{eff} but different scattering and absorption values were imaged to see if either μ_a or a modified value of the absorption coefficient is more suitable to use for the estimation of the optoacoustic signal strength in equation (2).

2.2. Phantoms

In order to fit in the transducer assembly of the Laser Optoacoustic Imaging System (LOIS), the phantoms were made of cylindrical shape with a diameter of 13 cm and a height of 6-7cm. Two different phantom materials were used.

The gelatin phantoms were made of 1 liter water which was heated up to 70-80℃. Afterwards 85g of Type-A-Gelatin from porcine skin (300 Bloom, Sigma, Cat.#G2500) was slowly stirred into the water. Once the gelatin was completely dissolved, 10ml homogenized milk (3.25% fat) was added to yield an effective optical attenuation coefficient μ_{eff} of approximately 1.30 cm^{-1}.[5] After pouring the solution into a mold and putting the targets into the liquid, the mold was stored in a refrigerator to solidify the phantom. Since the fragments in gelatin are known not to absorb in the near infrared (NIR), the absorption coefficient μ_a of the gelatin phantoms were assumed to be equivalent to that of water ($\mu_a \approx 0.13 cm^{-1}$ at 1064nm laser light).[13] Using equation (3) a reduced scattering coefficient μ_s' of $4.20 cm^{-1}$ for the gelatin phantoms was calculated.

The other type of phantoms were made of Polyvinyl Chloride-Plastisol (PVCP). The liquid plasticizing PVCP is mixed with a certain amount of black plastic color (BPC), an optical absorber, to yield the desired optical absorption value. Titanium dioxide (TiO_2) was added to yield the desired optical scattering values. For cooling and solidification, the liquid was poured in a cylindrical mold. The phantom preparation process is described in detail in elsewhere.[14,15] The empirical formulas used to calculate the optical coefficients were:

$$\frac{\mu_a}{cm^{-1}} = (12.818 \pm 0.001)\, A_{BPC} \tag{4}$$

$$\frac{\mu_{s'}}{cm^{-1}} = ((2.6 \pm 0.2)\frac{mL}{mg})\, S_{TiO_2} + (1.4 \pm 0.1) \tag{5}$$

where A_{BPC} is the percentage concentration of BPC by volume, and S_{TiO_2} is the concentration of TiO_2 in $\frac{mg}{mL}$. The optical properties of the phantom and target-material were not measured directly but only determined by equation (4) and (5).

Based on the previous equations, we were able to produce phantoms out of both materials (gelatin and PVCP) which had similar optical properties. Therefore differences in the optoacoustic signal between these phantoms at equal laser light illumination had to be due to mechanical properties (as expressed by Γ).

Tumor-mimicking targets with different optical properties were embedded in both types of phantoms. Table (1) shows a list of the phantoms made with embedded PVCP targets and their corresponding optical properties. The targets were all made of PVCP. Targets with shapes of a circle (surface area of 71mm^2), triangle and square, both with a surface area of 50mm^2, were embedded in phantom G0. These targets had a thickness of (7.0 ± 0.5)mm. The targets in all the other phantoms had cylindrical shape with a diameter of (9.5 ± 0.5)mm and a length of (25 ± 1)mm in phantom G1 and G2 and a length of (30 ± 1)mm in phantom P1. A schematic view of the target position inside the phantoms is shown in Figure (1). For the phantoms G1 and G2 the targets were placed closer to the center of the phantom. Due to geometrical arrangement of the transducers (creating a natural focus at the center), targets were better defined when placed at the phantom center.

Table 1. List of phantoms made (all values correspond to an illumination with 1064nm). Note that all of the targets were made with PVCP.

No.	**PHANTOM**				**TARGETS**			
	Material	μ_a / cm^{-1}	$\mu_{s'}$ / cm^{-1}	μ_{eff} / cm^{-1}	No.	μ_a / cm^{-1}	$\mu_{s'}$ / cm^{-1}	μ_{eff} / cm^{-1}
P1	PVCP	0.13	4.20	1.30	T1 T2 T3	0.17 0.50 0.86	1.40	0.89 1.69 2.41
G0	gelatin	0.13	4.20	1.30	T1-T3	0.5	1.4	1.69
G1	gelatin	0.13	4.20	1.30	T1 T2 T3	0.33 0.19 0.13	1.40 2.80 4.20	1.30
G2	gelatin	0.13	4.20	1.30	T1 T2 T3	0.13	1.40 2.80 4.20	0.77 1.07 1.30

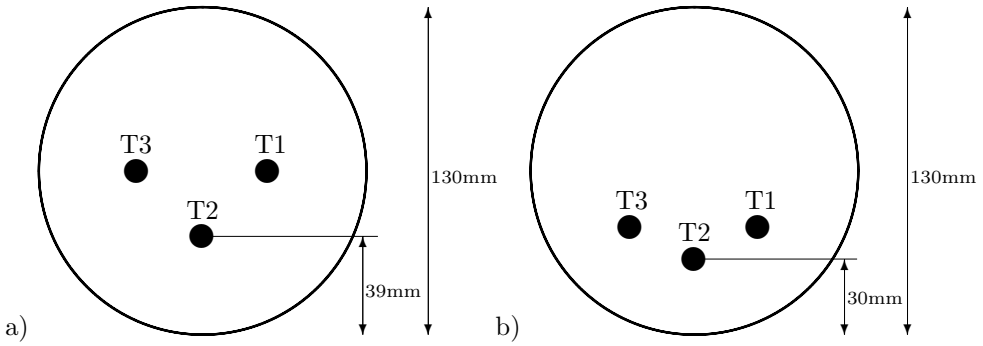

Figure 1. phantoms (from illuminated site) at reduced scale of 1:3
a) G1 and G2 b) G0 and P1

2.3. Thermal lesions in liver samples

In order to demonstrate the potential of optoacoustic imaging for the detection and characterization of thermal lesions in tissue, a bovine liver study was conducted. Thermal lesions were produced in ex vivo liver using a 805nm laser with an input power of 5W and an exposure duration of 600s. Optical fibers were used to couple the

laser light to the liver. Due to the low laser power used for imaging (see 2.4), the lesions were located directly under the liver surface so that the imaging laser light was not significantly attenuated before reaching the lesions. For a more reproducible localization of the lesions, the liver was embedded in a non scattering gelatin phantom without milk. On the other hand differences in the speed of sound in liver (1550m/s)[16] and gelatin (assumed to be water equivalent, 1485m/s)[17] may cause small image distortions due to the fact that the reconstruction algorithms assume a constant speed of sound throughout the entire imaging domain. Figure (2) shows a thermal lesion in one liver (a) and a liver with two lesions embedded in gelatin (b) respectively.

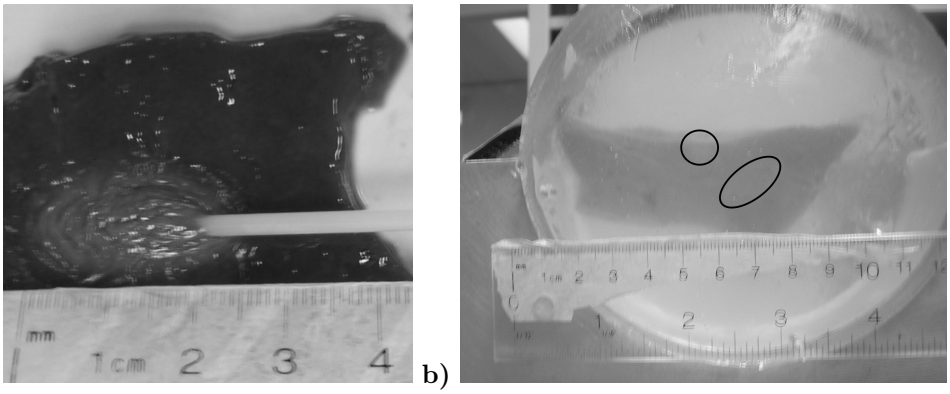

Figure 2. (a) A thermal lesion in bovine liver produced with 805nm laser, (b) liver embedded in gelatin during imaging (position of the lesions are marked)

2.4. Experimental Setup

Figure (3a) shows the experimental setup. A pulsed Nd:YAG laser (Qswitched, Quantel) with a wavelength of 1064nm, a pulse duration of 14ns and a 10Hz repetition rate was used to illuminate the samples. Locations with the same optical and thermoelastical properties, μ_a and Γ respectively, should yield the same optocoustic signal, provided that the fluence is the same over the entire phantom surface. To achieve a homogenous laser fluence distribution over the whole circular top surface of the phantom, the laser beam was expanded by two concave lenses with -50mm and -75mm focal length respectively. Use of these lenses decreased the laser fluence incident on the phantom surface to approximately $0.2mJ/cm^2$; this resulted in a weak optoacoustic signal to noise ratio. Phantom P1 was imaged with another LOIS system using higher fluence of approximately 20 mJ/cm^2. However, without the homogenous laser fluence distribution the optoacoustic signal at different locations inside the phantom would not be comparable. Figure (3b) shows gelatin phantom G0 (see Table 1) with targets of equal optical properties but different shapes (triangle, square, circle). They appear with almost similar contrast. Moreover, the resolution of the system enables the recognition of the target shapes.

For imaging, the phantom was placed on an acoustic transducer array which was oriented perpendicular to the optical path (see Figure 3a). The transducer array was comprised of 32 single ultra-wide band acoustic transducer elements positioned in a 165° arc formation with a diameter of 127mm. The single transducers were made of 100μm thick, 12mm length and a 1mm width polyvinylidene fluoride (PVDF) film. The produced ultrasound signals were detectable with the ultra-wide band transducers in a range from 50 kHz to 6 MHz.[5] An acoustic signal, produced at one point inside the phantom other than the center of the ultrasound array, is detected by every transducer at a slightly different time after the incident laser pulse due to the different distances between this point and the different single transducers. Every point of the phantom produces an acoustic signal whose strength depends on its optical and thermo-elastic properties. One single transducer detects an optoacoustic signal from every point inside the phantom. These time-resolved signals were amplified by the preamplifier placed in the transducer housing and a signal amplifier placed within the external hardware of LOIS. An average of 16 laser pulses were used to acquire the data and the amplified analog signal is converted into digital form at a sampling rate of 12MHz.[5] With the knowledge of the sound velocity in the media, distances can be calculated.

a) 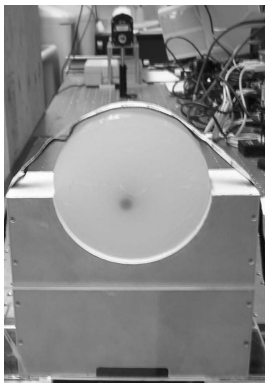 b) 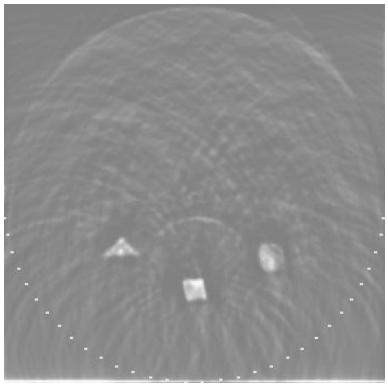

Figure 3. a) Experimental setup: transducer with a gelatin phantom in the front and laser with lenses in the background; b)Optoacoustic Image of G0 using LOIS software

The optoacoustic signal is filtered from low-frequency acoustic noise and high-frequency electrical noise, then integrated to produce values proportional to the velocity potential. A radial back-projection algorithm is used to reconstruct a two dimensional image from the integrated signals detected by all transducers in the arc-shaped array.[3] The LOIS also offers the option of normalizing the image intensity to incident laser fluence. The total time for data acquisition and image reconstruction is about 2 seconds.[7]

Different types of filters can be applied in order to remove image artefacts and optimize the signal to noise ratio by varying the used frequency band. For all images three different types of filters with different parameters were applied and the setting with the best image contrast and signal to noise ratio was chosen. Applying different filters with different parameters can change the image contrast. One filter option is the Finite Impulse Response filter (FIR), a bandpass-filter applied after Fourier-transformation from the time domain into frequency domain. Another option is a Boxcar filter, which is applied in the time-domain. The Wavelet filter reconstructs an image for each ultrasonic frequency separately and calculates the resulting image as sum of all these images. That algorithm improves the image especially if targets with different sizes are imaged.

Several parameters affect image brightness and its contrast to background. The radial back-projection method employed in the image reconstruction does not provide for quantitative comparison of target contrast. Hence, only qualitative comparisons can be made. We have, however, started to analyze the raw optoacoustic signal to provide for improved quantitative analysis of the image data.

3. EXPERIMENTAL RESULTS

3.1. Phantom studies - Optoacoustic image contrast

To demonstrate the potential effect of mechanical properties on image formation, phantoms were made that have the same optical properties but different mechanical properties. The imaging target in all cases was made of PVCP, whereas the background was made of gelatin or PVCP. The PVCP phantom P1 (Table 1, Figure 1) showed poor image contrast between targets and surrounding phantom-material (Figure 4a). This may be caused by the similarity of the Grüneisen parameter in equation (2) for the target and the background material. Thermo-acoustic properties were similar because targets and the surrounding media consist of the same material. The targets had differences only in optical properties from the surrounding material. Target T1 with optical absorption properties nearly similar to the phantom background (Table 1) achieved the worst contrast and is hardly visible in the optoacoustic image.

In contrast PVCP targets in the gelatin phantoms G1 and G2 with comparable optical properties as in the previous experiment with the PVCP phantom P1 (especially with target T1 from P1) showed better image contrast (Figure 4b and 4c), even though P1 had been illuminated with significantly higher laser fluence. As targets

and background in the gelatin phantoms vary in Γ, the materials differ in their speed of sound, heat capacity and thermal expansion coefficients. We posit that this leads to differences in ultrasonic wave-production between target and surrounding material and therefore results in a significant optoacoustic contrast despite similar optical absorption properties.

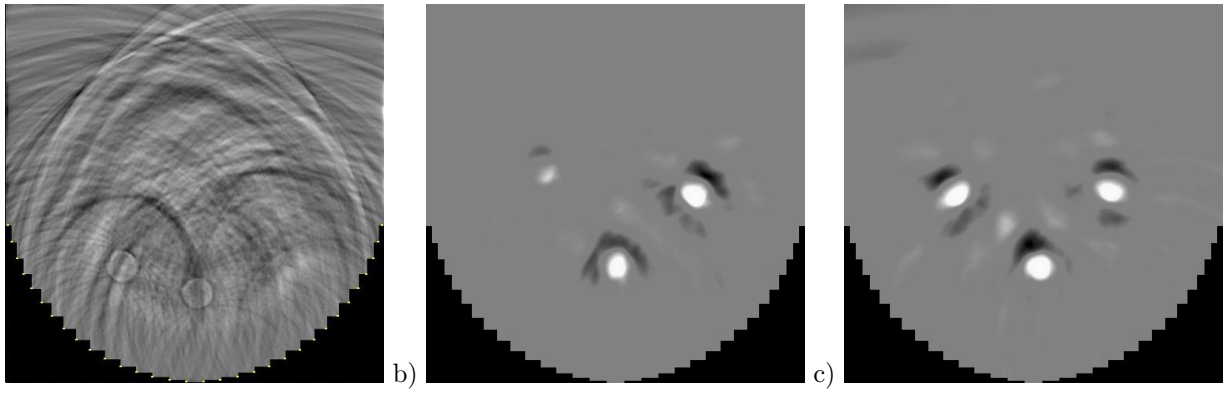

Figure 4. Optoacoustic images of a) P1 , b) G1 and c) G2 using LOIS software

Comparing the image contrast of targets embedded in G2 in Figure (4c) the experiments showed that targets with the same optical absorption coefficient μ_a, but different scattering properties $\mu_{s'}$, appeared with almost equal optical contrast. Targets with different optical absorption but equal effective absorption properties μ_{eff} in G1 (Figure 4b) appeared with different contrast in the optoacoustic image. Targets with high absorption of $\mu_a = 0.33\text{cm}^{-1}$ and low scattering of $\mu_{s'} = 1.40\text{cm}^{-1}$ yield a stronger optoacoustic signal than targets with low absorption $\mu_a = 0.13\text{cm}^{-1}$ and high scattering $\mu_{s'} = 4.20\text{cm}^{-1}$ although both targets have the same μ_{eff}. Therefore, the effect of scattering in the small targets compared to the large phantoms is negligible, so that μ_a represents the correct characteristic value for the optical contrast of targets in equation (2).

Figure (4b) also shows that targets with very small differences in optical absorption ($\mu_a^{T1} = 0.13\text{cm}^{-1}$ vs. $\mu_a^{T2} = 0.19\text{cm}^{-1}$ in phantom G1) compared to the background optical absorption were visualized. Also note that low optical absorption $\mu_a = 0.13 - 0.50\text{cm}^{-1}$ is sufficient to yield a strong optoacoustic signal in the gelatin phantoms G1 and G2. Although the contrast for these targets is not only caused by relative optical differences between target and phantom material, optical absorption is necessary for heating and expansion of the tissue. By yielding strong optoacoustic signals with these low absolute absorption values, the experiments demonstrated the high sensitivity of the transducer elements and the capabilities of optoacoustic imaging.

3.2. Optoacoustic imaging of thermal lesions

With the motivation to use optoacoustic imaging for the detection of thermal lesions, especially for real-time evaluation of prostate cancer thermal therapy, the capability of LOIS to detect thermal lesions was investigated. Previous experiments showed that, due to the low laser fluence (see section 2.4), lesions in liver tissue deeper than 1 cm under the surface, were very difficult to detect. Hence, surface thermal lesions were induced in liver and imaged. Figure (5) shows the optoacoustic image of the sample and a picture of the liver after it was removed from the gelatin.

The continuous arrows in Figure (5) point to the two marked lesions. Their position can be compared with the picture of the liver in Figure (5b) taken after imaging. We should note that due to insufficient laser fluence used in this experiment, the image contrast was poor. However, position and dimensions of thermal lesions have been detected. Immediately noticeable are the bright areas at the border of liver tissue and gelatin. This may be the result of differences in mechanical properties, i. e. acoustic impedance, such that one would expected the gelatin to more easily expand in a direction away from the liver. The different sound velocities between liver and gelatin could also influence the optoacoustic signal at the interface. Moreover, phantom fabrication

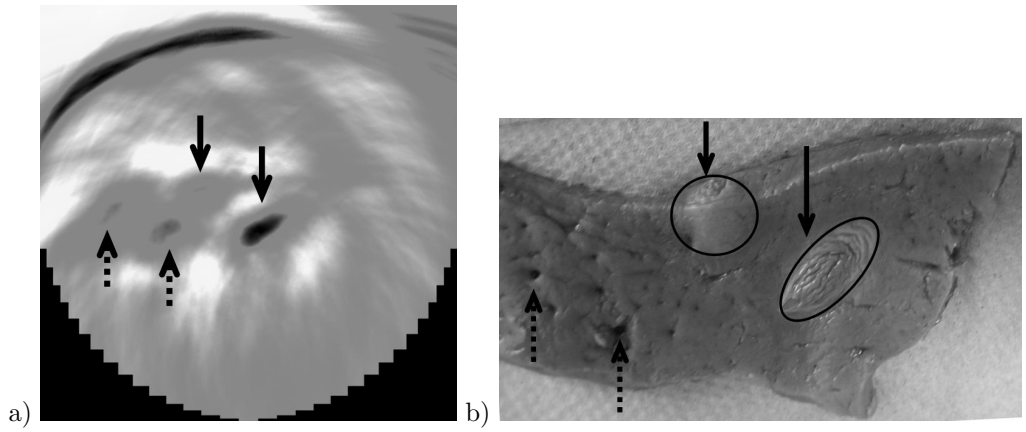

Figure 5. a) Optoacoustic image of liver sample embedded in gelatin (continuous arrows: thermal lesions, dashed arrows: blood vessels); b) liver sample after imaging in same orientation

which involved pouring hot liquid gelatin around the tissue sample may have partially coagulated the liver tissue. Comparing the pictures of the liver before and after imaging (Fig. 2 and 5 respectively) a change of the liver tissue color and density is apparent. The central region of bottom thermal lesion in Figure (5a) appears darker than the surrounding tissue, indicating a reduced optoacoustic signal. This may be the result of a heat-induced change in optical properties such that the optical fluence at the center of the lesions is reduced caused by strong attenuation of NIR light at 1064nm in the coagulated liver. Interestingly the thermal lesion at the top surface of the the liver was not visualized with good contrast. This may be a result of the proximity of this lesion to the gelatin-liver interface, such that the rather large signal generated at the boundary dominated. There are two additional dark regions in the image (dashed arrows) which can be assigned to blood vessel openings in the liver.

4. DISCUSSION

These experiments in tissue equivalent phantoms demonstrate that optoacoustic imaging is influenced not only by differences in optical absorption, but also in mechanical, thermoelastic properties. This is an important characteristic for real time monitoring of thermal therapies. Thermoelastic properties like the thermal expansion coefficient β, the speed of sound and the acoustic impedance, in general, are expected to change significantly by thermal coagulation. The thermal expansion coefficient of water for example has shown to have a strong temperature dependence, which has enabled the non-invasive calculation of temperature during heating.[18,19] Preliminary experiments showed that thermal lesion in liver tissue, ex vivo, can be visualized. Practical problems like inhomogeneities in the tissues, low laser power and coagulation caused by the hot gelatin will be addressed in subsequent experiments.

For quantitative interpretation of image contrast and signal amplitude, the fluence as a function of the illumination depth is required. Computer simulations, e.g. using a Monte-Carlo-algorithm, are necessary to calculate the fluence in rigid or inhomogeneous media. Also the influences of applying different filters or other post processing algorithms on image contrast need to be taken into account when comparing image contrast and quality. In future experiments, the thermal lesion will be imaged not only after thermal treatment but also before and during heating the tissue. Thereby the lesion and the coagulation of the tissue can be examined during treatment.

5. CONCLUSION

This preliminary study demonstrated that low optical absorption targets can be visualized using a 32 element optoacoustic imaging array. Furthermore, it was shown that image contrast was poorer when PVCP targets were embedded in a PVCP background phantom compared to a gelatin background phantom. This indicates that the Grüneisen parameter Γ, (i.e. mechanical properties) may play a more prominent role in the acoustic

signal generation than previously thought, such that a better understanding of this parameter is needed. Finally, it was demonstrated that the optoacoustic imaging array was able to detect a thermal lesion in ex vivo bovine liver, indicating the potential of this technique for monitoring thermal therapies.

ACKNOWLEDGMENTS

The authors would like to acknowledge Arthur Worthington for technical assistance, Dr. Sergey Ermilov for reimaging the PVCP phantom, Dr. Sebastian Brand for helpful conversations on ultrasound propagation and Robin Castelino for his help with post processing. The financial support of Ryerson University, the Canadian Foundation for Innovation, Natural Science and Engineering Research Canada and the German Academic Exchange Service is also gratefully acknowledged.

REFERENCES

1. V. Gusev and A. Karabutov, *Laser Optoacoustics*, American Institute of Physics, New York, 1992.
2. A. A. Oraevsky, S. L. Jacques, R. O. Esenaliev, and F. K. Kittel, "Time-resolved optoacoustic imaging in layered biological tissues," in *Advances in Optical Imaging and Photon Migration*, R. R. Alfano, ed., **21**, pp. 161–165, Academic Press, 1994.
3. A. A. Oraevsky and A. A. Karabutov, "Optoacoustic tomography," in *Biomedical Photonics Handbook*, T. Vo-Dinh, ed., **PM125**, ch. 34, pp. 34/1–34/34, CRC Press, 2003.
4. B. Colston Jr, U. Sathyam, L. DaSilva, and M. J. Everett, "Dental oct," *Optical Express* **3**, pp. 230–238, 1998.
5. G. M. Spirou, I. A. Vitkin, B. C. Wilson, W. M. Whelan, P. M. Henrichs, K. Mehta, T. Miller, A. Yee, J. Meador, and A. A. Oraevsky, "Development and testing of an optoacoustic imaging system for monitoring and guiding prostate cancer therapies," *Proc. SPIE* **5320**, pp. 44–56, July 2004.
6. A. A. Oraevsky, A. Karabutov, S. Solomatin, and et al., "Laser optoacoustic imaging of breast cancer in vivo," *Proc. SPIE* **4256**, pp. 6–15, June 2001.
7. V. G. Andreev, A. A. Karabutov, S. V. Solomatin, E. V. Savateeva, V. Aleynikov, Y. V. Zhulina, R. D. Fleming, and A. A. Oraevsky, "Opto-acoustic tomography of breast cancer with arc-array transducer," *Proc. SPIE* **3916**, pp. 36–47, May 2000.
8. V. G. Andreev, A. E. Ponomarev, M. M. P. M. Henrichs, E. Orihuela, E. Eyzaguirre, and A. A. Oraevsky, "Detection of prostate cancer with opto-acoustic tomography," *Proc. SPIE* **4960**, pp. 45–57, July 2003.
9. X. Wang, Y. Pang, G. Ku, X. Xie, G. Stoica, and L. V. Wang, "Noninvasive laser-induced photoacoustic tomography for structural and functional in vivo imaging of the brain," *Nature Biotechnology* **21**, pp. 803–806, July 2003.
10. G. Ku, X. Wang, X. Xie, G. Stoica, and L. V. Wang, "Imaging of tumor angiogenesis in rat brains in vivo by photoacoustic tomography," *Applied Optics* **44**, pp. 770–775, February 2005.
11. A. A. Oraevsky, S. Jacques, and F. Tittel, "Measurement of tissue optical properties by time-resolved detection of laser-induced transient stress," *Applied Optics* **36**, pp. 402–415, January 1997.
12. L. H. Wang and S. L. Jacques, *Monte Carlo Modeling of Light Transport in Multi-Layered Tissues in Standard C*, M. D. Anderson Cancer Center Press, Houston, Texas, 1993.
13. G. Hale and M. Querry, "Optical constants of water in the 200 nm to 200 m wavelength region," *Applied Optics* **12**, pp. 553–563, 1973.
14. G. M. Spirou, A. A. Oraevsky, I. Vitkin, and W. Whelan, "Optical and acoustic properties at 1064 nm of polyvinyl chloride-plastisol for use as a tissue phantom in biomedical optoacoustics," *Physics in Medicine and Biology* **50**, pp. N141–N153, 2005.
15. G. M. Spirou, "An investigation of pulsed and frequency domain photoacoustics and their applicability to biomedical studies," Master's thesis, Graduate Department of Medical Biophysics, University of Toronto, 2005.
16. "Lexikon der physik und technik in der medizin," in *Thieme, Leipzig, Germany*, Wilfried Angerstein, 1985.
17. P. Fish, *Physics and Instrumentation of Diagnostic Medical Ultrasound*. Willey, NY, USA, 1990.

18. K. V. Larin, I. V. Larina, M. Motamedi, and R. O. Esenaliev, "Optoacoustic laser monitoring of cooling and freezing of tissues," *Quantum Electronics* **32**, pp. 953–958, 2002.
19. I. V. Larina, K. V. Larin, and R. O. Esenaliev, "Real-time optoacoustic monitoring of temperature in tissues," *Journal of Physics D: Applied Physics* **38**, pp. 2633–2639, 2005.